*inorganics*

MDPI

*Article*

# Light Inorganic Scintillation Materials for Neutron and Charge Particle Detection

**Mikhail Korzhik [1,2,*], Ilia Komendo [1], Andrei Fedorov [1,2], Alexey Bondaray [2], Daria Kuznetsova [1], Vitaly Mechinsky [1,2] and Andrei Vasil'ev [3]**

[1] National Research Centre "Kurchatov Institute", 1 Kurchatov sq., 123098 Moscow, Russia; i.comendo@gmail.com (I.K.); andrei.fedorov@cern.ch (A.F.); daria_kyznecova@inbox.ru (D.K.); vitaly.mechinsky@cern.ch (V.M.)
[2] Institute for Nuclear Problems of Belarus State University, 11 Bobruiskaya, 220030 Minsk, Belarus; alesonep@gmail.com
[3] Skobeltsyn Institute for Nuclear Physics, Lomonosov Moscow State University 1(2), Leninskie Gory, GSP-1, 119991 Moscow, Russia; anvasiliev52@gmail.com
* Correspondence: mikhail.korjik@cern.ch

**Abstract:** The technological aspects of the light inorganic crystalline compounds suitable to create scintillation materials to detect charged particles and neutrons in a wide energy range have been examined. Among them, $Li_2CaSiO_4$:Eu was found to be a prospective candidate to control the valent state of the Rare Earth (RE) and to provide a high intensity of luminescence. It was demonstrated that the material has room for future improvement; however, this requires precise engineering of its composition—an experimental search of compositions or additives that will provide the maximum $Eu^{2+}/Eu^{3+}$ ratio to achieve a high scintillation light yield. The benefits of light inorganic materials are disclosed through the modeling of the linear density of nonequilibrium carriers along secondary particle tracks created in scintillators utilized for neutron detection. It is shown that oxide matrices have a larger linear density in comparison with halide crystalline compounds under alpha-particles and tritons, whereas light oxides can provide smaller numbers under protons.

**Keywords:** lithium calcium silicate; light crystalline compound; scintillator; europium; charged particle; ionization; density of nonequilibrium carriers



**Citation:** Korzhik, M.; Komendo, I.; Fedorov, A.; Bondaray, A.; Kuznetsova, D.; Mechinsky, V.; Vasil'ev, A. Light Inorganic Scintillation Materials for Neutron and Charge Particle Detection. *Inorganics* **2023**, *11*, 315. https://doi.org/10.3390/inorganics11080315

Academic Editor: Matteo Mauro

Received: 30 June 2023
Revised: 18 July 2023
Accepted: 23 July 2023
Published: 25 July 2023



## 1. Introduction

The scintillation method for measuring ionizing radiation [1] is widely used in a variety of fields, ranging from scientific research to radiography and medical imaging [2]. Simultaneously, the scope of their application is broadening, such as the requirement to measure neutrons with a wide range of energies, including those that are signatures of thermonuclear reactions that will be used in the future energy industry.

In fusion experiments with deuterium d and tritium t fuel, the major fusion reactions ($d + d$, $d + t$, $t + t$) involve the following neutron production channels [3].

$$\begin{array}{c} d + d \rightarrow {}^3He + n(2.45\ MeV) \\ d + t \rightarrow {}^4He + n(14.0\ MeV) \\ t + t \rightarrow {}^4He + n + n(0 - 8.8\ MeV) \end{array} \quad (1)$$

To date, a few inorganic scintillation detector media are used to detect neutrons based on isotopes of light elements ($^3$He, $^6$Li $^{10}$B), as well as heavy Gd [4–6] and U [7–9]. With the exception of gaseous helium, other elements can form inorganic crystalline compounds containing large concentrations (>$10^{22}$ cm$^{-3}$) of nuclei interacting with neutrons. A common disadvantage of the above light nuclei is the rapid decrease in the interaction cross section according to the law ~1/vn, where vn is the neutron speed. Their cross sections are reduced to bn units in the energy range of epithermal neutrons [10,11]. With an increase

in the energy of neutrons, new reaction channels open with the emission of both protons and α-particles [12]. The heavier nuclei of the elements Cl, O, Al, and Ga contribute the most to the interaction in this energy range. Table 1 shows the integrals of the neutron cross sections of the nuclei of individual isotopes of the listed elements for processes that open after a neutron energy of more than 8 MeV.

**Table 1.** Integral cross-sections of the nuclei of some isotopes of the elements creating the scintillation compounds [13].

| Isotope | Energy Range, MeV | Integral Cross-Section (*n*, *p*), bn | Integral Cross-Section (*n*, Total), bn |
|---|---|---|---|
| $^{35}$Cl | 1–20 | 1.66 | 45.7 |
| | 1–150 | >1.66 | 212.4 |
| $^{37}$Cl | 1–20 | >0.26 | 47.0 |
| | 1–150 | >0.26 | 220.0 |
| $^{69}$Ga | 1–20 | 0.439 | 65 |
| | 1–200 | 0.638 | 437 |
| $^{71}$Ga | 1–20 | 0.206 | 64.6 |
| | 1–200 | 0.387 | 437 |
| $^{27}$Al | 1–20 | 0.966 | 37.7 |
| | 1–150 | 0.966 | 198 |
| $^{16}$O | 1–20 | 0.302 | 30 |
| | 1–150 | 0.435 | 144 |

Evidently, the proton production cross-section is quite small and weakly dependent on energy, and the interaction products are dominated by α-particles, deutrons, and tritons.

A class of gadolinium-based garnet structure compounds for detecting neutrons in the thermal and epithermal energy ranges has been developed [14,15]. Gadolinium-based scintillation materials find applications for neutron detection, primarily due to the high neutron cross section of the natural mixture of gadolinium, equal to 46,000 bn for thermal neutrons. At the same time, due to the compound's high effective charge, these crystals have a relatively high sensitivity to γ-radiation [16]. There is an elpasolite-structured scintillation material family that has a unique set of parameters for neutron detection; however, mass production remains difficult [17,18].

Thus, there is a demand for light scintillation materials, where the detection of high-energy neutrons can be provided by the detection of the same kind of secondary particles, which are generated by the light nuclei under thermal and epithermal neutrons. Such a combination of atoms in a compound should ensure the detection of neutrons in a fairly wide energy range. Analyzing the genesis of the development of the technology of inorganic scintillation materials, we can say that the awareness of the advantages of light inorganic compounds appeared more than 20 years ago [19–21]. A noticeable interest in them grew with the start of research on a wider set of the light materials for the purpose of creating scintillators for neutron detection [22–25]. The range of activating additives was expanded, and work was also carried out to combine several elements (Li, B, O) containing nuclei that effectively interact with neutrons [26,27].

An ideal crystalline matrix to detect neutrons in a wide energy range would be $^{6}$LiCl. It combines $^{6}$Li to absorb thermal neutrons, whereas chlorine isotopes $^{35,37}$Cl provide an interaction with fast neutrons. However, this material is quite hygroscopic and is useless for doping with rare-earth ions. Nevertheless, its attractiveness led to the development of a series of eutectic crystalline combinations, which include lithium chloride and a compound allowing doping with 2+ and 3+ rare-earth ions [28,29]. At the same time, light compounds

with a scintillation yield comparable to the relatively heavy LiI(Eu) or elpasolites have not yet been obtained.

Recently, $Li_2CaSiO_4$:Eu (LCS) was demonstrated to be a bright scintillator to construct neutron sensitive screens [30]. It has a low $Z_{eff}$ ~ 15, which predetermines a low sensitivity to background γ-quanta. It contains light and middle-light elements as well as a small amount of the element europium with a high neutron resonance integral [31]. Aside from its polycrystalline form, it can also be grown in a single-crystalline form [32], potentially broadening the application area of $Li_2CaSiO_4$:Eu. A performance of a screen sample with 180 μm thickness and an area of 160 $mm^2$ in comparison to the commercially available Scintacor ND screen ($^6$LiF-ZnS:Ag) was evaluated under the neutron radiation of a Pu-Be source with an activity of $4.7 \times 10^4$ neutron/s and a γ-radiation source $^{137}$Cs with a total activity of $9 \times 10^3$ $s^{-1}$ ($7.6 \times 10^3$ $s^{-1}$ of 662 keV γ-quanta) [33]. It was demonstrated that the new scintillator provides a high neutron detection efficiency with a reduced screen thickness. Therefore, the sensitivity to the high-energy γ-quanta, particularly those of 4.4 MeV, will be reduced.

Let us compare lithium-containing crystalline materials in terms of the following parameters: density, which is correlated with $Z_{eff}$; the volume concentration of lithium; and the possibility of isovalent localization of activator rare-earth (RE) ions. A comparison of the parameters of the typical compounds is given in Table 2. The structure data and densities of the compounds were taken from the database [34], and the amounts of lithium atoms were calculated.

**Table 2.** Parameters of some light lithium-containing crystalline inorganic materials.

| Compound | Structure, Spatial Symmetry | Li Atoms/$cm^3$ | Density, g/$cm^3$ |
|---|---|---|---|
| $Li_2CaSiO_4$ | Tetragonal, $I\bar{4}2m$. Consists of $LiO_4$ trigonal pyramids, $SiO_4$ tetrahedra, and $CaO_8$ polyhedra. | $2.3 \times 10^{22}$ | 2.86 |
| γ-$LiAlO_2$ | Tetragonal, $P4_{\bar{1}}2_{\bar{1}}2_{\bar{1}}$. Consists of $LiO_4$, and $SiO_4$ tetrahedra. | $2.4 \times 10^{22}$ | 2.64 |
| $LiYO_2$ | Monoclinic, $P2_1/c$. $Li^+$ is bonded in a distorted T-shaped geometry to three $O^{2-}$ atoms. $Y^{3+}$ is bonded to six $O^{2-}$ atoms to form a mixture of distorted corner and edge-sharing $YO_6$ octahedra. | $1.9 \times 10^{22}$ | 4.10 |
| $LiYSiO_4$ | Monoclinic, $P2_1/c$. Consists of $LiO_5$ trigonal bipyramids, $YO_7$ pentagonal bipyramids, and $SiO_4$ tetrahedra. | $1.1 \times 10^{22}$ | 3.65 |
| $LiAlSiO_4$ | Trigonal, R3. Consists of $LiO_4$, $AlO_4$ и $SiO_4$ tetrahedra. | $1.2 \times 10^{22}$ | 2.69 |
| $Li_3AlMO_5$ (M = Al, Ge, Ga) | Orthorhombic, $Pna2_1$. Stannite structure. Consists of $LiO_4$, $AlO_4$, $GeO_4$, and $GaO_4$ tetrahedra. | $2.7 \times 10^{22}$ | 3.08–4.2 |
| $LiCaAlF_6$ | Trigonal, $P\bar{3}1c$. Consists of $LiF_6$, $CaF_6$, $SiF_6$ octahedra | $9 \times 10^{21}$ | 2.86 |

The listed compounds can be doped with 3d-ions. Compared to such activator ions, RE ions provide a higher light yield in scintillators due to the participation of mixed electronic states of df configurations in an energy exchange with the exciton subsystem of nonequilibrium carriers and, as a rule, have faster scintillation kinetics (with the exception of the $Tb^{3+}$ ion, which has scintillation kinetics of the order of milliseconds). However, RE ions preferentially localize in octahedral and higher oxygen coordinations; therefore, not every type of crystal lattice is suitable for doping a compound with RE ions.

Compounds having Li and Y ions in the matrices are the heaviest in the list. From the standpoint of a combination of physico-chemical properties, the compounds $Li_2CaSiO_4$ and $Li_3AlMO_5$ (M = Al, Ge, Ga) may be distinguished. The $Li_3AlSiO_5$ compound is a deep-ultraviolet nonlinear optical crystal [35], but the entire class of materials is only suitable for 3d-element doping.

In this article, we focused on studying the potential for the future improvement of the $Li_2CaSiO_4$:Eu scintillation properties. Of particular interest was a comparison of LCS neutron-sensitive material with other species for the detection of the secondary particles created by neutrons. The materials were examined for ionization density, which regulates the light yield, as invented by Birks [36].

The $Li_2CaSiO_4$ compound is suitable for doping with divalent ions, providing isovalent substitution of Ca ions. This is quite difficult to manage in compounds where no appropriate site for defect-less substitution exists [37]. Nevertheless, Li-based compounds have a tendency to defect formation in the anion sublattice, which contributes to the stabilization of heterovalent impurity ions in different valence states. That is, the stabilization of europium ions predominantly in the divalent state in lithium compounds is a separate and interesting problem of inorganic chemistry.

## 2. Results and Discussion

### *2.1. Photoluminescence Study of Eu-Doped Scintillator $Li_2CaSiO_4$ and Possibilities for Light Yield Enhacement*

Europium, even under the condition of isovalent substitution, is localized in inorganic compounds both in 3+ and 2+ valence states. It is known that, for $Li_2CaSiO_4:Eu^{2+}$, the luminescence intensity depends on the ratio of $Eu^{2+}$ and $Eu^{3+}$, which is formed during high-temperature synthesis due to the volatilization of a part of lithium, resulting in the formation of cation vacancies in the crystal lattice, the charge compensation of which occurs due to the appearance of the Schottky pair $V'_{Li} + \frac{1}{2}V_{\ddot{O}}$ [38]. Under such conditions, the probability of luminescence quenching of $Eu^{2+}$ ions increases both due to the interaction with quenching centers based on electron traps and the nonradiative transfer to $Eu^{3+}$ ions. We compared two methods of preferential stabilization of Eu ions in the divalent state in $Li_2CaSiO_4$. First, light cations were used to nonisovalently replace silicon ions. Some of the $Si^{4+}$ ions in the compound were replaced by $Al^{3+}$ ions, as described in [39]. This procedure creates negatively charged vacancies in the crystal structure, which prevent the oxidation of $Eu^{2+}$ to $Eu^{3+}$. Another method was to substitute a part of the $SiO_2$ tetrahedra with the $Si_3N_4$ polyhedra. This method was used to boost the brightness of $Li_2MSiO_4:Eu^{2+}$ phosphors, where M stands for Ca, Sr, and Ba [40]. Figure 1 compares the luminescence intensity of LCS samples obtained by two methods. Samples with nonisovalent substitution of aluminum ions for silicon ions demonstrated a twofold increase in luminescence intensity, while the $Li_2CaSiO_{2.5}N$:Eu compound showed an almost threefold increase in intensity compared to $Li_2CaSiO_4:Eu^{2+}$. At the same time, the photoluminescence spectra recorded at 395 nm excitation show the bands of both $Eu^{2+}$ and $Eu^{3+}$ ions. They depict a significant decrease in the luminescence intensity of $Eu^{3+}$ ions at the nonisovalent substitution of $Si^{4+}$ by $Al^{3+}$ ions. In the nitrogen co-doped sample, no $Eu^{3+}$ luminescence bands were observed at all.

It is worth noting that a significant increase in the luminescence intensity is not accompanied by a similar increase in the scintillation yield. For the $Li_2CaSiO_{2.5}N$:Eu samples, it turned out to be even smaller than for $Li_2CaSiO_4:Eu^{2+}$ at the same activator concentrations. This indicates that the concentration of nonisovalent additives requires additional fine tuning to prevent an increase in lattice point defects, which are, as a rule, electron traps.

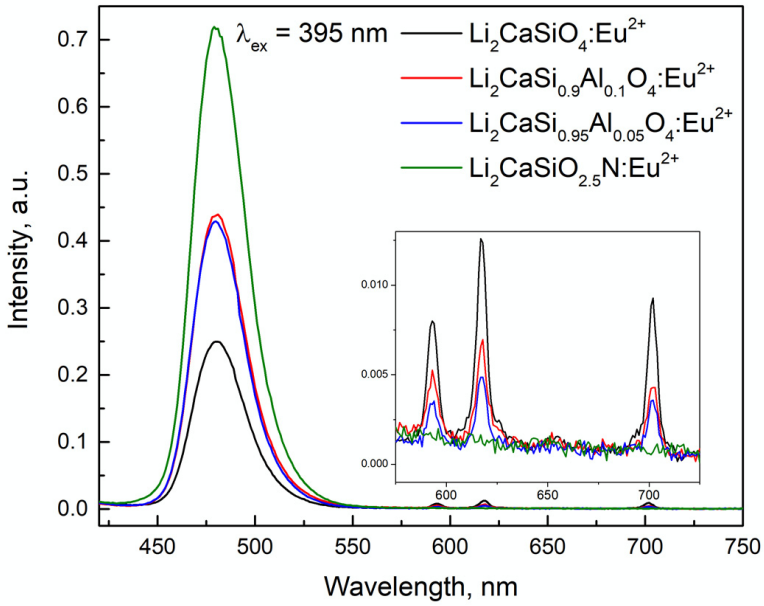


**Figure 1.** Photoluminescence spectra of $Li_2CaSiO_4:Eu^{2+}$ samples in comparison with samples with nonisovalent substitution of $Si^{4+}$ by $Al^{3+}$ ions, and $Li_2CaSiO_{2.5}N$:Eu registered at excitation wavelength of 395 nm.

It is important to note that, even in a polycrystalline form, lithium calcium silicate forms sufficiently large transparent crystallites (Figure 2). It might be crucial in terms of light extracting when LCS will be used as a component of neutron-sensitive coatings.

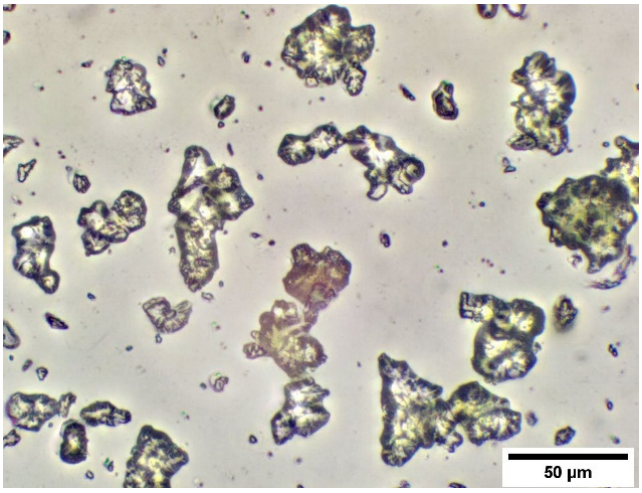


**Figure 2.** Optical microscopy in the transmitted light of particles of the $Li_2CaSiO_4$:Eu.

*2.2. Evaluation of Various Scintillators for Charged Particles Detection*

The ability of the material to separate α-particles of different energies is the most important factor in detecting secondary heavy charged particles formed by neutrons of different energies. Since the charged particles under consideration are not relativistic, the major energy losses are due to ionization. At the same time, the energy resolution in a simplistic form, as in the case of γ-quanta, is formed by three factors: the scintillation yield, material properties that determine the internal resolution of the material, and the track fluctuations of both the secondary particle itself and ionized electrons [41]. Although fluctuations are smaller in denser materials, the increased sensitivity to background γ-quanta becomes a significant factor, limiting their use for secondaries' detection. Internal resolution is also a significant factor. For the registration of α-particles, one of the best

inorganic scintillation materials with a low internal resolution is $YAlO_3$:Ce (YAP) [42]. However, this material is not sensitive to low-kinetic-energy neutrons. The yield of material scintillations for neutron detection should be considered in relation to the $\alpha/\gamma$ factor. A high scintillation yield with a low $\alpha/\gamma$ factor of the scintillator will provide overlap between the $\alpha$-particles and background $\gamma$-ray signals.

The light yield of the scintillator correlates to the density of pairs of nonequilibrium carriers formed in the track. The average linear density of nonequilibrium carriers can be estimated as $<N_{pairs}>/dx = <dE/dx>/(\beta E_g)$. Using a computer simulation, we estimated ionization losses $<dE/dx>$ of various charged particles: electrons, protons, $\alpha$-particles, and tritium nuclei (tritons) in bulk of widespread scintillators such as LSO ($Lu_2SiO_5$), CLYC ($CsLiYCl_6$), NaI:Tl, YAP ($YAlO_3$:Ce), and the new promising material LCS ($Li_2CaSiO_4:Eu^{2+}$). The results of the simulation are presented in Figure 3. The average specific energy losses $<dE/dx> = E_0/<l_{tr}>$ were calculated using the primary energies $E_0$ and $<l_{tr}>$.

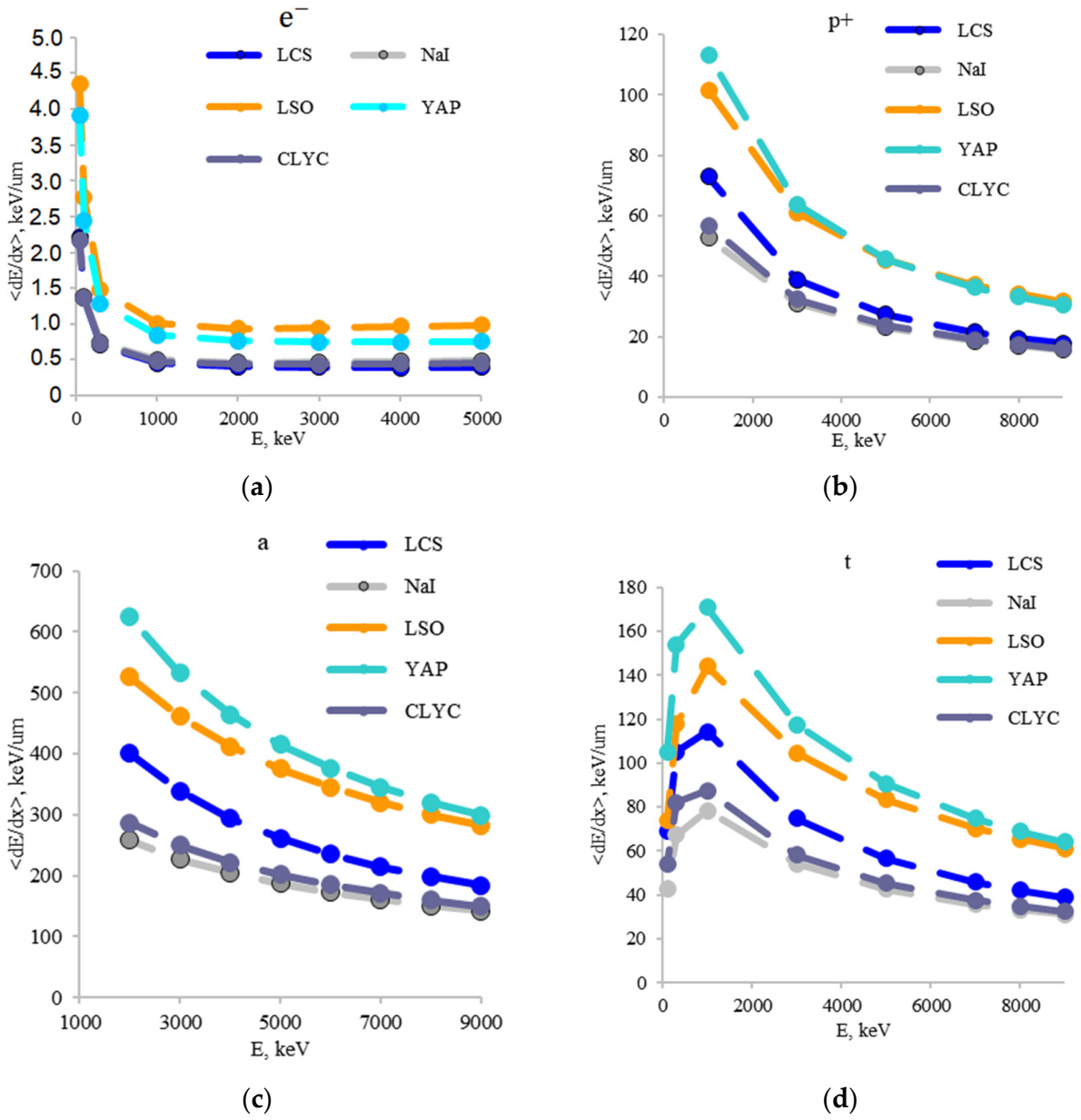


**Figure 3.** Ionization losses of electrons (**a**), protons (**b**), $\alpha$-particles (**c**), and tritons (**d**) in several scintillation materials.

The positions of the specific energy losses' curves follow the change of the density of the material in the case of electrons; the heavier a material is, higher ionization losses occur. As expected, the specific losses for the heavier charged particles are significantly high. However, the positions of their curves are reshuffled. Apparently, the result that oxides exhibit average specific energy losses greater than the halide compounds is determined by a high electron density in oxides.

The choice of the conversion efficiency parameter of the material ($\beta$) requires more detailed comment. This parameter is the ratio between the average energy $E_{eh}$ required to create one electron-hole pair and the bandgap of the material, which is equal to the minimum energy of such a pair. The value of $\beta$ characterizes the efficiency of the multiplication cascade of electronic excitations in the scintillation material [43,44]. When interacting with the electron subsystem, an electron can only create a new pair if the energy conservation law is fulfilled in the process $e \rightarrow 2e + h$, and thus the kinetic energy of an electron must be greater than the bandgap. Similarly, the creation of a new electron-hole pair in the Auger process for holes $h \rightarrow 2h + e$ will occur only if the hole is at least $E_g$ below the top of the valence band. When secondary electron-hole pairs are created, secondary electrons and holes will be distributed in energy in the first approximation proportionally to the density of states (DOS). Thus, it is necessary to estimate the average energy of electrons in the region where they cannot create secondary pairs, the so-called "passive" region, with kinetic energies from zero to the multiplication threshold. In addition, one more relaxation process has to be taken into account. Relaxation by phonons occurs in parallel with the multiplication process at electron energies slightly above the threshold energy. The phonon emission probability can be quite high near the multiplication threshold and leads to a loss of carrier energy with a further transition to the "passive" region. The competition of relaxation channels causes the multiplication threshold to shift to higher energies. As an example, Figure 4 shows the densities of states in an NaI and YAP crystal (calculated by the DFT method and given in the AFLOWLIB.ORG repository [45]). Note that YAP is interesting for consideration because its $E_g$ value was found to be different on the simulation model applied [46]. The yellow curves correspond to the passive region, and the blue curves correspond to the extended passive region, taking into account the shift in the effective manifestation of the multiplication threshold by 2 eV. The average kinetic energy of electrons and holes calculated from these passive regions is also shown in the figures.

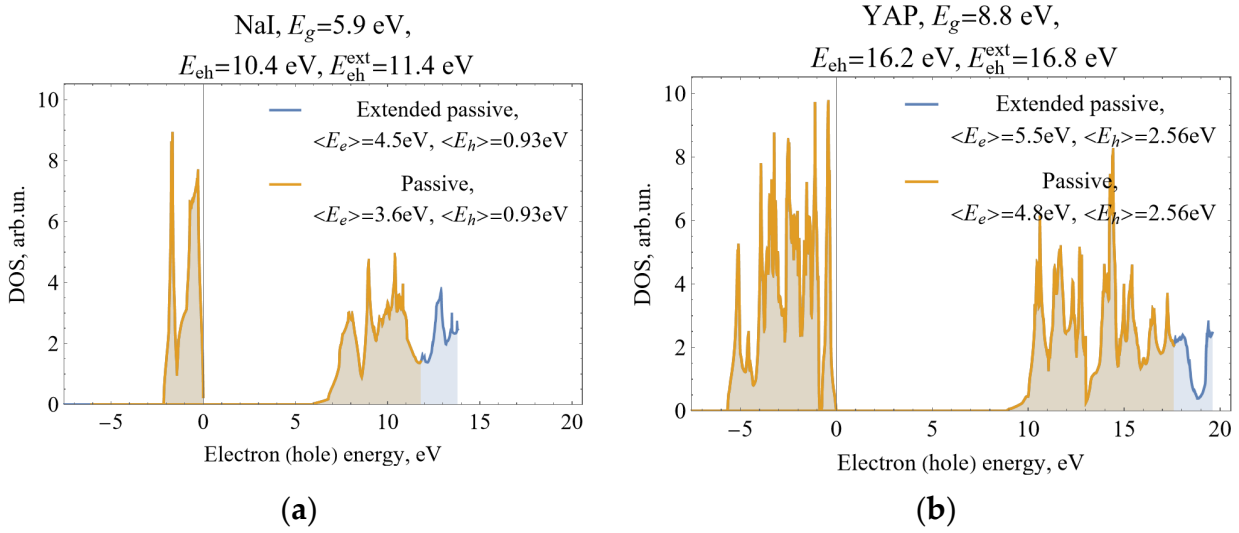


**Figure 4.** Distribution of density of states in NaI (**a**) and YAP (**b**).

The average energy required to create one pair is $E_{eh} = E_g + \langle E_e \rangle + \langle E_h \rangle$. As seen, the value of $\beta = E_{eh}/E_g$ depends on several factors: the electronic structure of the material,

and the strength of the electron–phonon interaction, which in turn depends on the ionicity of the crystal. For ionic crystals, the rate of energy loss of carriers for the emission of polarization optical photons is much higher than the corresponding rate in covalent crystals with deformation optical phonons. Figure 5 depicts the estimated values of a few materials based on the relaxation processes taken into account. Note that for a number of materials, the additional features of the electronic structure can significantly change the β value compared to the given simple estimate. For instance, the proximity of the 5pCs core level to the Auger process threshold for holes in CsI can significantly reduce the estimate of β [47].

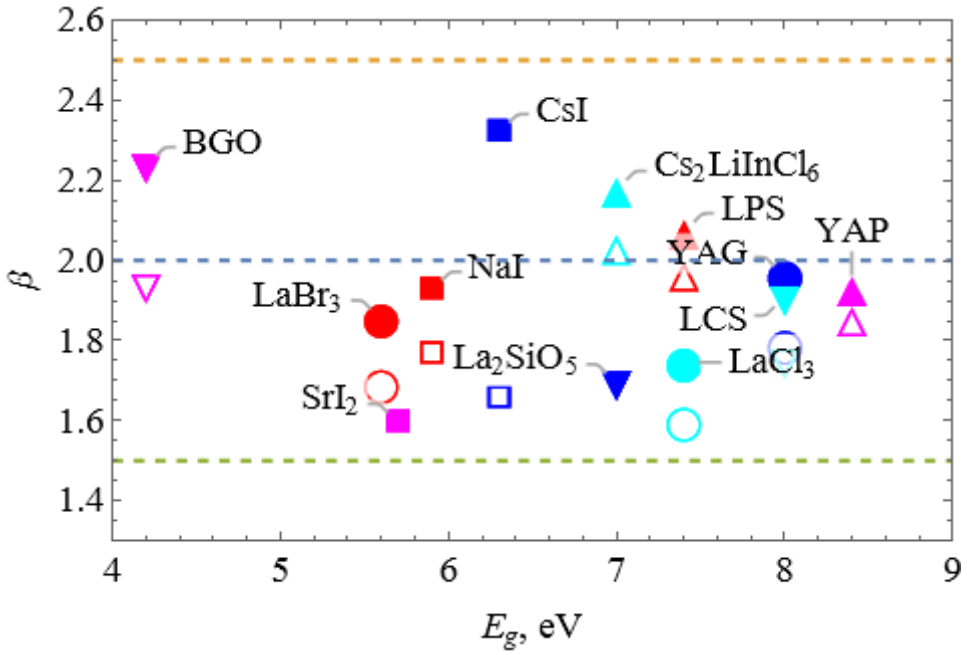


**Figure 5.** Spread of β values for some inorganic materials. Filled symbols correspond to the passive regions expanded due to relaxation on phonons, in which the multiplication of electronic excitations is impossible; open symbols correspond to the multiplication threshold equal to the band gap.

The following bandgap values $E_g$ of the compounds were used to calculate the average linear density of nonequilibrium carriers: LSO—6.2 eV, YAP—7.8 eV, LCS—5.2 eV, NaI—5.9 eV, and CLYC—4.9 eV. In addition, taking into account considerations of the $\beta$ factor by authors [48–50], the following values of β were used for evaluation: LSO—2.5, YAP—2.5, LCS—2.5, NaI—1.7, and CLYC—2.

Figure 6 depicts the estimated dependence of the average linear density of nonequilibrium carriers on the energy of secondary particles.

For electrons and the lightest secondary particles (protons), the trend in the arrangement of the curves is preserved, as shown in Figure 3. The average linear density of nonequilibrium carriers for alpha particles and tritons is nearly equal for NaI(Tl) and LCS, whereas it is significantly higher for the other materials. It can be noted that the transverse dimensions of the track will also be smaller in heavier materials. Apparently, a smaller track volume implies a higher density of exciton states and, consequently, a stronger effect of the mutual quenching of excitons. This process competes with the capture of excitons by activator ions and, as a consequence, leads to a decrease in the scintillation yield. In this context, europium-activated scintillators have an advantage for detecting secondary particles, since they allow a large concentration of the activator in the crystalline compound.

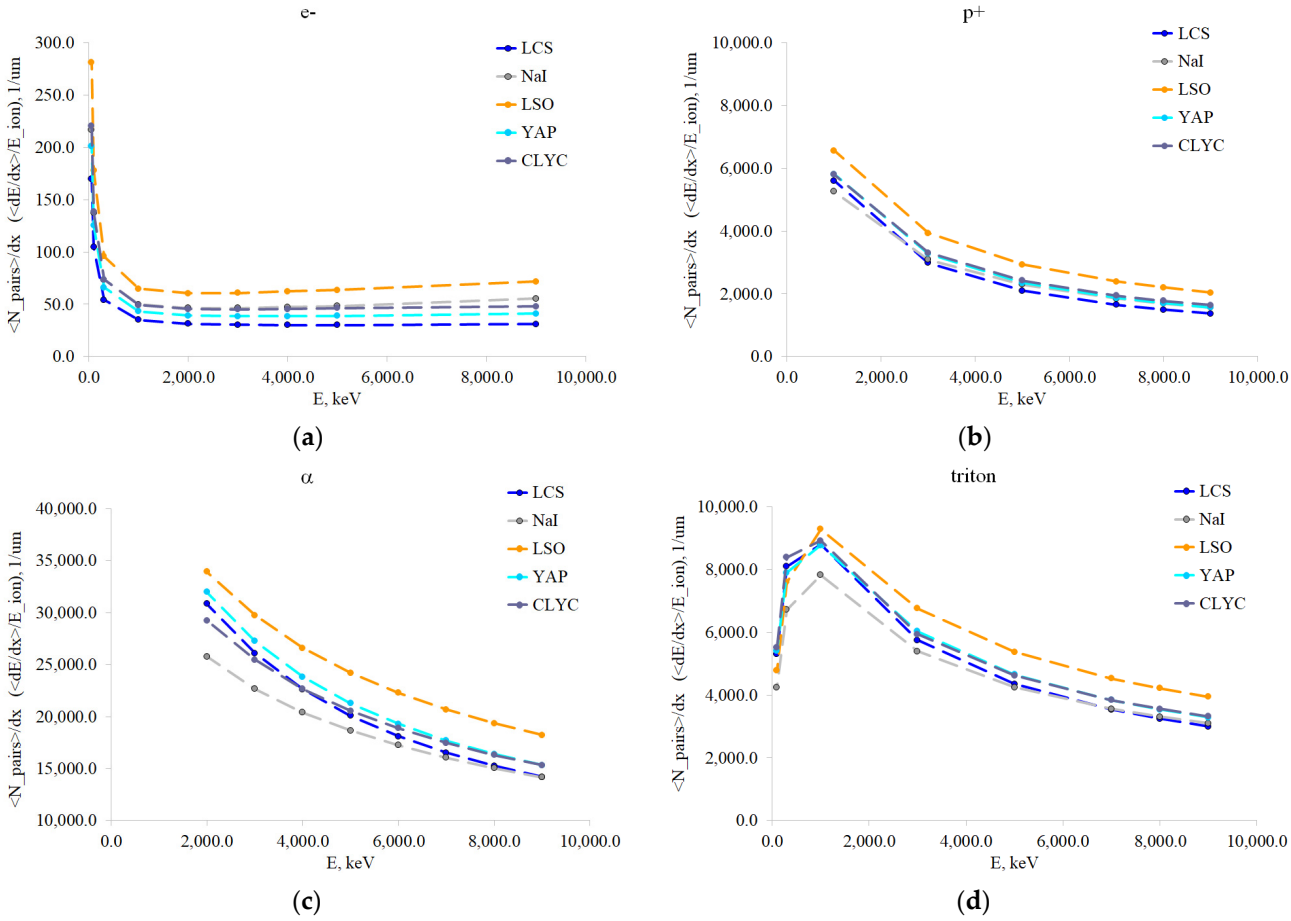


**Figure 6.** Energy dependence of the average linear density of nonequilibrium carriers created in several scintillation materials under electrons (**a**), protons (**b**), α-particles (**c**), and tritons (**d**).

## 3. Materials and Methods

### *3.1. Samples Synthesis*

The method for producing the polycrystalline compound $Li_2CaSiO_4$:Eu is described elsewhere [30,33]. Samples of LCS co-doped with aluminum or nitrogen were prepared by a variety of the sol-gel method. Acidic hydrolyzed tetraethyl orthosilicate was used as a source of $SiO_2$. In obtained silica-sol sociometric amounts of reagent grade $Li_2CO_3$, $CaCO_3$, $Eu_2O_3$, and $Al(NO_3)_3$ corresponding to a composition of $Li_2Ca_{0.998}Eu_{0.002}Si_{1-x}Al_xO_4$ (x = 0.05, 0.1) were added. Formed gel was dried at 100 °C, comminuted by mortar and pestle, and sieved through a 150-mesh sieve. The powder was calcined at 850 °C during 2 h to release all $CO_2$. Then, the powder was comminuted again and sieved. In a case of nitrogen co-doping, a necessary amount of $Si_3N_4$ for the composition $Li_2Ca_{0.998}Eu_{0.002}SiO_{2.5}N$ was added at this step. The reduction of $Eu^{3+}$ to $Eu^{2+}$ and the final synthesis of LCS were carried out in a tube furnace under a 5% $H_2$ + 95% $N_2$ atmosphere at 900 °C for 2 h.

### *3.2. Photoluminescence Measurements*

Photoluminescence spectra were recorded on a Fluorat-Panorama (LCC "Lumex", St. Petersburg, Russia) instrument using an excitation with a high-pressure xenon lamp operating in the short pulse mode (1 μs) with a repetition rate of 25 Hz.

### *3.3. Modeling and Simulation Procedure*

In modelling, we focused on the study of ionization losses in the track of various types of secondary particles (protons, alpha particles, and tritons) formed under the neutrons. These parameters were compared with similar ones for electrons that are generated in

materials due to the photo-absorption of γ-quanta. The evaluation was made using the GEANT4.10.0 software package [51]. The following compounds were selected for evaluation: NaI(Tl,) CLYC ($CsLiYCl_6$), YAP, LSO ($Lu_2SiO_5$), and LCS. Sodium iodide, in which part of the sodium is substituted for the lithium, is an attractive material for detecting neutrons [52]. CLYC has a high neutron detection yield. YAP and LSO oxygen compounds were chosen as materials with significantly different $\alpha/\gamma$ factors [53] and effective charges.

The following geometrical model was chosen for the simulation: a sphere of material with a diameter of 100 mm, in the center of which particles are emitted isotropically. For the energy value of each type of particle, $10^5$ particles were launched. When the energy decreased below the threshold of 100 eV, the length of the traversed track $l_{tr}$ was determined. The obtained value was plotted on the histogram of track lengths. An approximation of this curve yielded the average track length, $<l_{tr}>$.

## 4. Conclusions

In this work, in the consideration of scintillation materials, the emphasis is on those that make it possible to detect neutrons in a wide energy range. A particular focus is placed on the discussion of the properties of the light crystalline lithium-containing materials in order to select a crystal that combines high lithium content and the ability to stabilize rare earth activator ions in the valent state of the interest in this matrix. It has been found that in oxide light matrices of lithium-silica compounds, europium ions can be stabilized predominantly in the divalent state. Technological methods for such stabilization are considered; luminescent measurements confirm the possibility of minimizing the concentration of $Eu^{3+}$ ions in the $Li_2CaSiO_4$ compound. Technological methods to increase the intensity of $Eu^{2+}$ photoluminescence have been examined. Nonisovalent substitution in cation and anion sub-lattices was investigated. Both were found to be prospective; however, to increase the yield of scintillations, their certain refinement is required, especially from the point of view of establishing sufficiently accurate ratios between the concentrations of europium and nonisovalent dopants. The described technological methods for the stabilization of $Eu^{2+}$ in this matrix open the door for the creation of the $Li_2CaSiO^4$:$Eu^{2+}$ compound in a single-crystal form.

The developed material was compared with other materials occasionally used to detect neutrons and not only gamma-rays and charged particles. To compare the materials for the registration of secondary particles, the energy dependence of the average linear density of nonequilibrium carriers were compared. Peculiarities of the formation of thermalized pairs in various types of compounds are considered. It is shown that the major uncertainty in the determination of the average linear density of nonequilibrium carriers is introduced by the uncertainty in the estimate of the conversion efficiency parameter of the material. The specific energy losses of heavy secondary particles were found to be significantly greater than those of electrons produced by photo-absorption in scintillators.

The average linear density of nonequilibrium carriers created in several scintillation materials under electrons was compared to the average linear density of secondary particles created in scintillation materials under neutrons, namely protons, α -particles, and tritons. Alkali-halides, such as NaI, show minimal losses for the heaviest secondary particles: alpha particles and tritons. From this point of view, they can provide a high yield of scintillations at the detection of thermal neutrons with a partial substitution of Na ions by Li ions in the matrix. For the lighter secondary particles, protons, it is shown that the lighter the complex oxides are, the lower the average linear density of nonequilibrium carriers, which might be caused by the appropriate change of electron density in the oxides considered. This provides better conditions for an effective energy transfer from the matrix excitonic states to activator ions at the latter's relatively high concentrations in the compound.

**Author Contributions:** Conceptualization, M.K., I.K. and A.V., Methodology M.K., V.M. and A.V., software A.V., Investigation A.F., I.K., A.B., V.M. and A.V., resources A.B., V.M. and A.V., Data curation I.K., D.K., V.M. and A.V., writing—original draft preparation I.K., M.K. and A.V., writing—review and editing I.K., M.K., D.K. and A.V., supervision D.K. and M.K., project administration D.K., funding acquisition I.K. and D.K. All authors have read and agreed to the published version of the manuscript.

**Funding:** This research received no external funding.

**Data Availability Statement:** Not applicable.

**Acknowledgments:** Authors at NRC "Kurchatov Institute" acknowledge support by the grant of NRC "Kurchatov institute" (№84 dated 20.01.2023). Authors from Moscow State University and Belarus State University are grateful for the support of the Russian Science Foundation Project No. 23–42-10005 and the Belarus Foundation for the Foundation for Fundamental Research F23-RSF-074.

**Conflicts of Interest:** The authors have no conflict of interest to disclose.

## References

1. Lecoq, P.; Gektin, A.; Korzhik, M. *Inorganic Scintillators for Detector Systems*; Particle Acceleration and Detection; Springer International Publishing: Cham, Switzerland, 2017. [CrossRef]
2. Wang, Z.; Dujardin, C.; Freeman, M.S.; Gehring, A.E.; Hunter, J.F.; Lecoq, P.; Liu, W.; Melcher, C.L.; Morris, C.L.; Nikl, M.; et al. Needs, Trends, and Advances in Scintillators for Radiographic Imaging and Tomography. *arXiv* **2022**, arXiv:2212.10322. [CrossRef]
3. Ericsson, G. Advanced Neutron Spectroscopy in Fusion Research. *J. Fusion EnergY* **2019**, *38*, 330–355. [CrossRef]
4. Murray, R.B. Use of $^{6}$LiI(Eu) as a Scintillation Detector and Spectrometer for Fast Neutrons. *Nucl. Instrum.* **1958**, *2*, 237–248. [CrossRef]
5. Knitel, M.J.; Dorenbos, P.; de Haas, J.T.M.; van Eijk, C.W.E. $LiBaF_3$, a Thermal Neutron Scintillator with Optimal n-$\gamma$ Discrimination. *Nucl. Instrum. Methods Phys. Res. Sect. A Accel. Spectrometers Detect. Assoc. Equip.* **1996**, *374*, 197–201. [CrossRef]
6. van Eijk, C.W.E.; Bessière, A.; Dorenbos, P. Inorganic Thermal-Neutron Scintillators. *Nucl. Instrum. Methods Phys. Res. Sect. A Accel. Spectrometers Detect. Assoc. Equip.* **2004**, *529*, 260–267. [CrossRef]
7. Knoll, G.F. *Radiation Detection and Measurement*, 4th ed.; John Wiley & Sons: New York, NY, USA, 2010.
8. Fadil, M.; Blandin, C.; Christophe, S.; Déruelle, O.; Fioni, G.; Marie, F.; Mounier, C.; Ridikas, D.; Trapp, J.P. Development of Fission Micro-Chambers for Nuclear Waste Incineration Studies. *Nucl. Instrum. Methods Phys. Res. Sect. A Accel. Spectrometers Detect. Assoc. Equip.* **2002**, *476*, 313–317. [CrossRef]
9. Galli, G.; Hamrita, H.; Kirkpatrick, M.J.; Odic, E.; Jammes, C. A New Discriminating High Temperature Fission Chamber Filled with Xenon Designed for Sodium-Cooled Fast Reactors. *Nucl. Instrum. Methods Phys. Res. Sect. A Accel. Spectrometers Detect. Assoc. Equip.* **2020**, *968*, 163947. [CrossRef]
10. Emrich, W. Chapter 5—Basic Nuclear Structure and Processes. In *Principles of Nuclear Rocket Propulsion*; Emrich, W., Ed.; Butterworth-Heinemann: Oxford, UK, 2016; pp. 55–80. [CrossRef]
11. Zhou, C.; Melton, A.G.; Burgett, E.; Hertel, N.; Ferguson, I.T. Neutron Detection Performance of Gallium Nitride Based Semiconductors. *Sci. Rep.* **2019**, *9*, 17551. [CrossRef]
12. CINDRO, N. A Survey of Fast-Neutron Reactions. *Rev. Mod. Phys.* **1966**, *38*, 391–446. [CrossRef]
13. NNDC | National Nuclear Data Center. Available online: https://www.nndc.bnl.gov/ (accessed on 14 February 2023).
14. Taggart, M.; Nakohostin, M.; Sellin, P. Investigation into the potential of GAGG:Ce as a neutron detector. *Nucl. Instrum. Methods Phys. Res. Sect. A Accel. Spectrometers Detect. Assoc. Equip.* **2019**, *931*, 121–126. [CrossRef]
15. Reeder, P.L. Neutron detection using GSO scintillator. *Nucl. Instrum. Methods Phys. Res. Sect. A Accel. Spectrometers Detect. Assoc. Equip.* **1994**, *340*, 371–378. [CrossRef]
16. Reeder, P.L. Thin GSO scintillator for neutron detection. *Nucl. Instrum. Methods Phys. Res. Sect. A Accel. Spectrometers Detect. Assoc. Equip.* **1994**, *353*, 134–136. [CrossRef]
17. Combes, C.M.; Dorenbos, P.; van Eijk, C.W.E.; Krämer, K.W.; Güdel, H.U. Optical and Scintillation Properties of Pure and $Ce^{3+}$-Doped $Cs_2LiYCl_6$ and $Li_3YCl_6$:$Ce^{3+}$ Crystals. *J. Lumin.* **1999**, *82*, 299–305. [CrossRef]
18. van Loef, E.V.D.; Dorenbos, P.; van Eijk, C.W.E.; Krämer, K.W.; Güdel, H.U. Scintillation and Spectroscopy of the Pure and $Ce^{3+}$-Doped Elpasolites: $Cs_2LiYX_6$ (X = Cl, Br). *J. Phys. Condens. Matter* **2002**, *14*, 8481. [CrossRef]
19. Pierron, L.; Kahn-Harari, A.; Viana, B.; Dorenbos, P.; van Eijk, C.W.E. X-Ray Excited Luminescence of Ce:$Li_2CaSiO_4$, Ce:$CaBPO_5$ and Ce:$LiCaPO_4$. *J. Phys. Chem. Solids* **2003**, *64*, 1743–1747. [CrossRef]
20. Pejchal, J.; Fujimoto, Y.; Chani, V.; Moretti, F.; Yanagida, T.; Nikl, M.; Yokota, Y.; Beitlerova, A.; Vedda, A.; Yoshikawa, A. Crystal Growth and Luminescence Properties of Ti-Doped $LiAlO_2$ for Neutron Scintillator. *J. Cryst. Growth* **2011**, *318*, 828–832. [CrossRef]
21. Fujimoto, Y.; Kamada, K.; Yanagida, T.; Kawaguchi, N.; Kurosawa, S.; Totsuka, D.; Fukuda, K.; Watanabe, K.; Yamazaki, A.; Yokota, Y.; et al. Lithium Aluminate Crystals as Scintillator for Thermal Neutron Detection. *IEEE Trans. Nucl. Sci.* **2012**, *59*, 2252–2255. [CrossRef]

22. Dickens, P.T.; Marcial, J.; McCloy, J.; McDonald, B.S.; Lynn, K.G. Spectroscopic and Neutron Detection Properties of Rare Earth and Titanium Doped $LiAlO_2$ Single Crystals. *J. Lumin.* **2017**, *190*, 242–248. [CrossRef]
23. Yanagida, T.; Fujimoto, Y.; Koshimizu, M.; Kawano, N.; Okada, G.; Kawaguchi, N. Comparative Studies of Optical and Scintillation Properties between $LiGaO_2$ and $LiAlO_2$ Crystals. *J. Phys. Soc. Jpn.* **2017**, *86*, 094201. [CrossRef]
24. Thoř, T.; Rubešová, K.; Jakeš, V.; Kučerková, R.; Pejchal, J.; Nikl, M. Titanium-Doped LiAlO2 Ceramics for Neutron Scintillation. *J. Phys. Conf. Ser.* **2022**, *2413*, 012015. [CrossRef]
25. Takizawa, Y.; Kamada, K.; Yoshino, M.; Yajima, R.; Kim, K.J.; Kochurikhin, V.V.; Yoshikawa, A. Growth of $^6$Li-Enriched $LiCl/BaCl_2$ Eutectic as a Novel Neutron Scintillator. *Jpn. J. Appl. Phys.* **2022**, *61*, SC1038. [CrossRef]
26. Havlíček, J.; Rubešová, K.; Jakeš, V.; Kučerková, R.; Beitlerová, A.; Nikl, M. Basic Study of Ceramic Lithium Strontium Borates as Thermal Neutron Scintillators. *J. Am. Ceram. Soc.* **2022**, *105*, 4039–4045. [CrossRef]
27. Jakeš, V.; Havlíček, J.; Průša, F.; Kučerková, R.; Nikl, M.; Rubešová, K. Translucent $LiSr_4(BO_3)_3$ Ceramics Prepared by Spark Plasma Sintering. *Ceram. Int.* **2022**, *48*, 15785–15790. [CrossRef]
28. Kutsuzawa, N.; Takizawa, Y.; Kamada, K.; Yoshino, M.; Kim, K.J.; Murakami, R.; Shoji, Y.; Kochurikhin, V.V.; Yoshikawa, A. Growth and Scintillation Properties of Eu-Doped $LiCl/Li_2SrCl_4$ Eutectic Scintillator for Neutron Detection. *J. Cryst. Growth* **2021**, *576*, 126373. [CrossRef]
29. Sasaki, R.; Kamada, K.; Kim, K.J.; Yajima, R.; Yoshino, M.; Kutsuzawa, N.; Murakami, R.; Horiai, T.; Yoshikawa, A. Fabrication of $CeCl_3/LiCl/CaCl_2$ Ternary Eutectic Scintillator for Thermal Neutron Detection. *Crystals* **2022**, *12*, 1760. [CrossRef]
30. Komendo, I.; Mechinsky, V.; Fedorov, A.; Dosovitskiy, G.; Schukin, V.; Kuznetsova, D.; Zykova, M.; Velikodny, Y.; Korjik, M. Effect of the Synthesis Conditions on the Morphology, Luminescence and Scintillation Properties of a New Light Scintillation Material $Li_2CaSiO_4:Eu^{2+}$ for Neutron and Charged Particle Detection. *Inorganics* **2022**, *10*, 127. [CrossRef]
31. Lee, J.; Hori, J.; Nakajima, K.; Sano, T.; Lee, S. Neutron Capture Cross Section Measurements of 151,153Eu Using a Pair of C6D6 Detectors. *J. Nucl. Sci. Technol.* **2017**, *54*, 1046–1057. [CrossRef]
32. Sharonov, M.Y.; Bykov, A.B.; Petričević, V.; Alfano, R.R. $Cr^{4+}$-Doped $Li_2CaSiO_4$ Crystal: Growth and Spectroscopic Properties. *Opt. Commun.* **2004**, *231*, 273–280. [CrossRef]
33. Komendo, I.; Bondarev, A.; Fedorov, A.; Dosovitskiy, G.; Gurinovich, V.; Kazlou, D.; Kozhemyakin, V.; Mechinsky, V.; Mikhlin, A.; Retivov, V.; et al. New scintillator $^6Li_2CaSiO_4:Eu^{2+}$for neutron sensitive screens. *Nucl. Instrum. Methods Phys. Res. Sect. A Accel. Spectrometers Detect. Assoc. Equip.* **2023**, *1045*, 167637. [CrossRef]
34. Jain, A.; Ong, S.P.; Hautier, G.; Chen, W.; Richards, W.D.; Dacek, S.; Cholia, S.; Gunter, D.; Skinner, D.; Ceder, G.; et al. The Materials Project: A materials genome approach to accelerating materials innovation. *APL Mater.* **2013**, *1*, 011002. [CrossRef]
35. Zhang, C.F.; Liu, L.; Lei, B.; Dong, X.; Yang, Z.; Li, H.; Pan, S. $Li_3AlSiO_5$: The First Aluminosilicate as a Potential Deep-ultraviolet Nonlinear Optical Crystal with the Quaternary Diamond-like Structure. *Phys. Chem. Chem. Phys.* **2015**, *18*, 4362–4369. [CrossRef]
36. Birks, J.B. (Ed.) Front Matter. In *The Theory and Practice of Scintillation Counting*; International Series of Monographs in Electronics and Instrumentation; Pergamon: Oxford, UK, 1964; p. iii. [CrossRef]
37. Taikar, D.; Tamboli, S.; Dhoble, S. Synthesis and photoluminescence properties of $Li_2SO_4$:RE (RE = $Eu^{3+}$, $Tb^{3+}$, $Gd^{3+}$ and $Ce^{3+}$) phosphors. *Optic* **2017**, *139*, 111–122. [CrossRef]
38. Jianming, Z.; Zhao, W.; Lan, L.; Wang, J.; Chen, J.; Wang, N. Enhanced Emission from $Li_2CaSiO_4:Eu^{2+}$ Phosphors by Doping with $Y^{3+}$. *J. Alloys Compd.* **2014**, *592*, 213–219. [CrossRef]
39. Retivov, V.; Dubov, V.; Komendo, I.; Karpyuk, P.; Kuznetsova, D.; Sokolov, P.; Talochka, Y.; Korzhik, M. Compositionally Disordered Crystalline Compounds for Next Generation of Radiation Detectors. *Nanomaterials* **2022**, *12*, 4295. [CrossRef]
40. Kim, D.; Ji, C.W.; Lee, J.; Bae, J.-S.; Hong, T.E.; Ahn, S.I.; Chung, I.; Kim, S.-J.; Park, J.-C. Highly Luminous $N^{3-}$-Substituted $Li_2MSiO_{4-\delta}N_{2/3\delta}:Eu^{2+}$ (M = Ca, Sr, and Ba) for White NUV Light-Emitting Diodes. *ACS Omega* **2019**, *4*, 8431–8440. [CrossRef]
41. Gektin, A.; Vasil'ev, A.N.; Suzdal, V.; Sobolev, A. Energy Resolution of Scintillators in Connection With Track Structure. *IEEE Trans. Nucl. Sci.* **2020**, *67*, 880–887. [CrossRef]
42. Barishevsky, V.G.; Korzhik, M.V.; Bogatko, A.P. $YAlO_3:Ce^{3+}$ scintillator for the spectrometry of α-particles. *Beloruss. Acad. Proc. Phys.* **1992**, *2*, 5. (In Russian)
43. Korzhik, M.; Tamulaitis, G.; Vasil'ev, A.N. *Physics of Fast Processes in Scintillators*; Particle Acceleration and Detection; Springer International Publishing: Cham, Switzerland, 2020. [CrossRef]
44. Gektin, A.; Vasil'ev, A. Scintillation, Phonon and Defect Channel Balance, the Sources for Fundamental Yield Increase. *Funct. Mater.* **2016**, *23*, 183–190. [CrossRef]
45. Curtarolo, S.; Setyawan, W.; Wang, S.; Xue, J.; Yang, K.; Taylor, R.H.; Nelson, L.J.; Hart, G.L.W.; Sanvito, S.; Buongiorno-Nardelli, M.; et al. AFLOWLIB.ORG: A Distributed Materials Properties Repository from High-Throughput Ab Initio Calculations. *Comput. Mater. Sci.* **2012**, *58*, 227–235. [CrossRef]
46. Piskunov, S.; Gopejenko, A.; Pankratov, V.; Isakoviča, I.; Ma, C.-G.; Brik, M.G.; Piasecki, M.; Popov, A.I. First Principles Calculations of Atomic and Electronic Structure of $Ti^{3+}$Al- and $Ti^{2+}$Al-Doped $YAlO_3$. *Materials* **2021**, *14*, 5589. [CrossRef]
47. Vasil'ev, A.N. Microtheory of Scintillation in Crystalline Materials. In *Engineering of Scintillation Materials and Radiation Technologies*; Korzhik, M., Gektin, A., Eds.; Springer Proceedings in Physics; Springer International Publishing: Cham, Switzerland, 2017; pp. 3–34. [CrossRef]
48. Rodnyi, P.A.; Dorenbos, P.; van Eijk, C.W.E. Energy Loss in Inorganic Scintillators. *Phys. Status Solidi (b)* **1995**, *187*, 15–29. [CrossRef]

49. Dorenbos, P. Fundamental Limitations in the Performance of $Ce^{3+}$, $Pr^{3+}$, and $Eu^{2+}$ Activated Scintillators. *IEEE Trans. Nucl. Sci.* **2010**, *57*, 1162–1167. [CrossRef]
50. Ronda, C.; Wieczorek, H.; Khanin, V.; Rodnyi, P. Review—Scintillators for Medical Imaging: A Tutorial Overview. *ECS J. Solid State Sci. Technol.* **2015**, *5*, R3121. [CrossRef]
51. Agostinelli, S.; Allison, J.; Amako, K.; Apostolakis, J.; Araujo, H.; Arce, P.; Asai, M.; Axen, D.; Banerjee, S.; Barrand, G.J.; et al. Geant4—A simulation toolkit. *Nucl. Instrum. Methods Phys. Res. Sect. A Accel. Spectrometers Detect. Assoc. Equip.* **2003**, *506*, 250–303. [CrossRef]
52. Menge, P.R.; Yang, K.; Ouspenski, V. Large Format Li Co-Doped Nai:Tl (Nail™) Scintillation Detector for Gamma-Ray and Neutron Dual Detection. In Proceedings of the 12th Pacific Rim Conference on Ceramic and Glass Technology: Ceramic Transactions, Waikoloa, HI, USA, 21–26 May 2017. [CrossRef]
53. Wolszczak, W.; Dorenbos, P. Nonproportional Response of Scintillators to Alpha Particle Excitation. *IEEE Trans. Nucl. Sci.* **2017**, *64*, 1580–1591. [CrossRef]